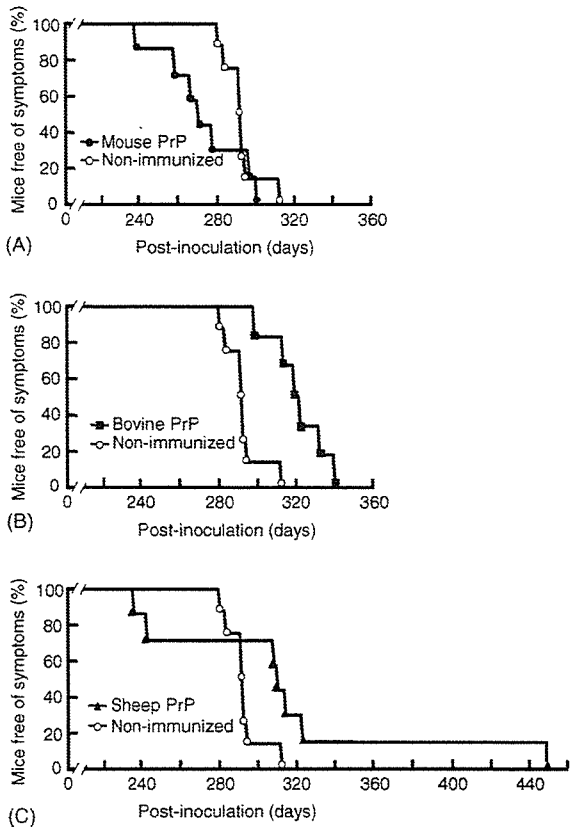

Fig. 1. Incubation times in mice immunized with mouse (A), bovine (B), and sheep (C) recombinant PrPs after intraperitoneal inoculation of a mouse-adapted Fukuoka-1 prion. (A) Incubation times in mice immunized with mouse recombinant PrP ($n=7$) and in non-immunized mice ($n=8$). No prophylactic effect from immunization with mouse recombinant PrP was detected. Instead, incubation times seemed to be shortened, compared with those of non-immunized mice. (B) Incubation times in mice immunized with bovine recombinant PrP ($n=6$) and in non-immunized mice ($n=8$). The immunized mice developed the disease with significantly delayed onset ($p=0.0008$, Logrank test). (C) Incubation times in mice immunized with sheep recombinant PrP ($n=7$) and in non-immunized mice ($n=8$). Except for two of the immunized mice, the other five mice showed extended incubation times compared to non-immunized mice.

the immunized mice 1 week after the final immunization. Non-immunized BALB/c mice developed the disease 291 ± 10 days post-inoculation (p.i.) (Fig. 1). Immunization with mouse recombinant PrP had no prophylactic effect against the disease. The immunized-mice succumbed to the disease at 269 ± 22 days p.i. (Fig. 1A). No significant difference in the incubation times could be detected between the mice immunized with and without mouse recombinant PrP ($p=0.22$, Logrank test), but incubation times of the immunized mice appeared to be shortened compared with those of the non-immunized mice. In contrast, mice immunized with recombinant bovine PrP showed significantly delayed onsets at 322 ± 15 days p.i., compared with non-immunized mice ($p=0.0008$, Logrank test, Fig. 1B). Immunization with recombinant sheep PrP showed variable effects against the prion. Five out of seven immunized mice developed the disease with prolonged onset (Fig. 1C). Two remaining mice became sick at 239 and 246 days p.i., as early as mice immunized with mouse recombinant PrP began to succumb (Fig. 1C). Accumulation of PrP^{Sc} and pathological changes including vacuolation and gliosis were indistinguishable in the brains of terminally diseased mice (data not shown).

3.2. *Bovine and sheep but not mouse recombinant PrP stimulates antibody responses against respective immunogens in mice*

To assess the immunogenicity of recombinant bovine, sheep, and mouse PrPs in mice, we investigated antibody responses in the immunized mice. Antisera were collected just before prion infection and each serum of the four to five immunized mice of each group was subjected to an ELISA to detect specific IgG antibodies against respective immunizing recombinant PrPs. In the mice immunized with mouse recombinant PrP, only slightly higher antibody binding expressed as optical density values at 405 nm (OD_{405}) were detected, compared with those of non-immunized mice (Fig. 2A). In contrast, much higher OD_{405} values were observed in the mice immunized with recombinant bovine and sheep PrPs (Fig. 2A). We also performed Western blotting of COS-7 cells transiently expressing mouse, sheep, and bovine PrP^{C} without a 6× His tag using the antisera. No mouse PrP^{C} could be detected by the anti-mouse recombinant PrP sera on Western blotting (Fig. 2B). In contrast, all of the anti-sheep and -bovine recombinant PrP sera we used for Western blotting substantially detected sheep and bovine PrP^{C} expressed in COS-7 cells, respectively (Fig. 2B). However, the signals were variable in intensity with each anti-sheep or -bovine recombinant PrP serum. Three out of four anti-bovine PrP sera showed relatively strong signals of bovine PrP^{C} but the remaining one exhibited faint signals (Fig. 2B). In the case of anti-sheep PrP sera, one antiserum revealed relatively strong signals but the remaining ones exhibited weak signals (Fig. 2B). These results indicate that recombinant bovine and sheep but not mouse PrP were immunogenic but their immunogenicities were variable in BALB/c mice.

We further carried out fluorescence activated cell sorter (FACS) analyses and found that the antisera against bovine and sheep PrPs also contained various amounts of antibodies capable of reacting with respective native PrP^{C} transiently expressed on COS-7 cells (Fig. 2C).

3.3. *Anti-PrP autoantibodies are variably produced in mice immunized with recombinant bovine and sheep PrPs*

We investigated whether the antisera against recombinant bovine and sheep PrPs could crossreact with mouse PrP by carrying out ELISA. The immunizing recombinant PrPs contained a 6× His tag. Therefore, to eliminate immunoreactivity

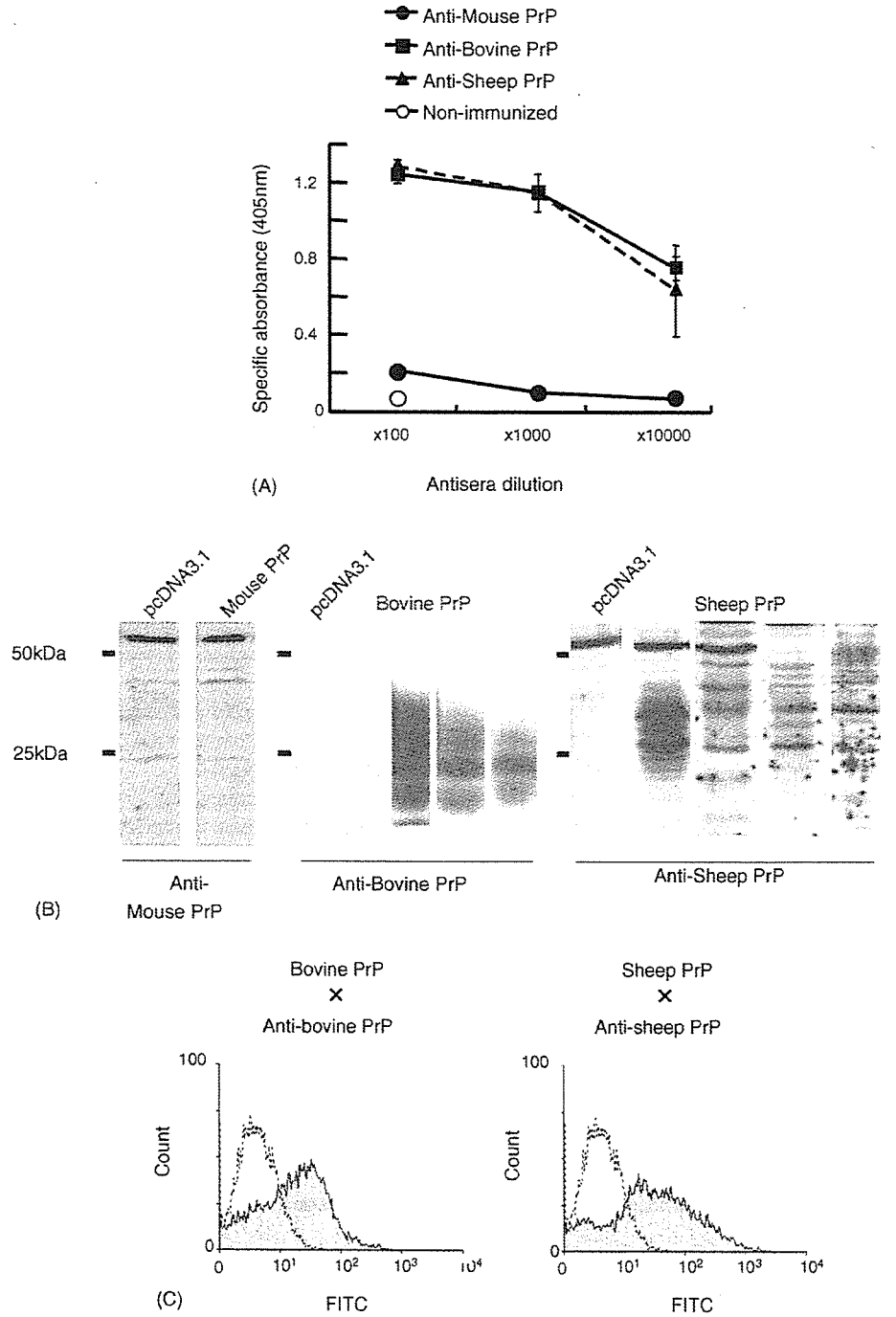

Fig. 2. Antibody responses in mice immunized with mouse, bovine, and sheep recombinant PrPs against the respective immunogens. (A) Each group of at least five mice was intraperitoneally immunized with the purified recombinant PrPs five times at 2-week intervals and anti-PrP IgG antibodies were detected in each serum of the immunized four to five mice of each group by an ELISA against the immunizing antigens. For anti-mouse PrP antibody detection, purified mouse recombinant PrP without a 6× His tag was used instead. (B) Antigenic specificities of each antiserum of the four immunized mice from each bovine and sheep recombinant PrP group were also examined by Western blotting of COS-7 cells transiently transfected with pcDNA3.1 vector alone or with pcDNA3.1 encoding each PrP^C. (C) FACS analysis of COS-7 cells transiently expressing each PrP^C. The cells transfected with the vector alone (unshaded) and the vector encoding bovine or sheep PrP^C (shaded) were probed by each antiserum.

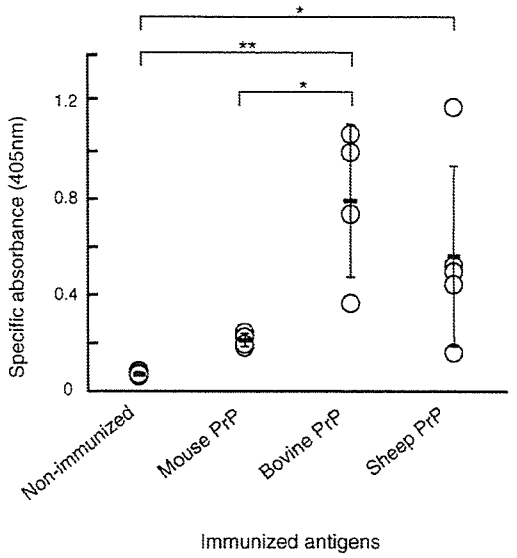

Fig. 3. Anti-PrP autoantibodies in mice immunized with recombinant mouse, bovine, and sheep PrPs. Each antiserum from four to five mice immunized with respective recombinant PrPs was diluted 1:100 and subjected to ELISA against purified mouse recombinant PrP without a 6× His tag. $^{*}p<0.05$; $^{**}p<0.01$.

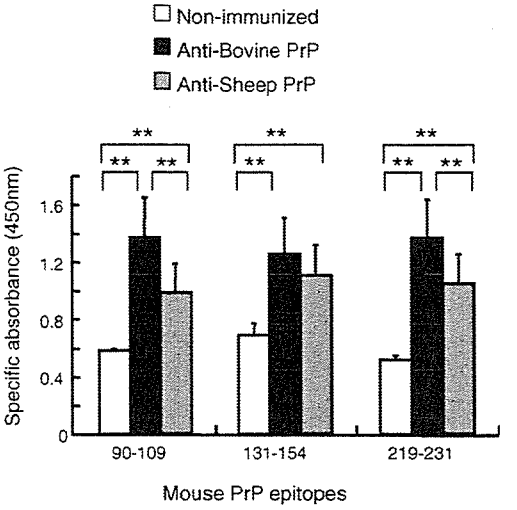

Fig. 4. Recognition of three different mouse PrP epitopes by antisera raised against bovine and sheep recombinant PrPs. The antisera used were collected from four to five mice of each immunization group. Mouse PrP peptides, moPrP90–109, moPrP131–154, and moPrP219–231, positively reacted with antisera raised against bovine and sheep recombinant PrPs on ELISA, compared with sera from non-immunized normal mice ($^{**}p<0.01$).

against the tag with antibodies that might be produced in the immunized mice, we used recombinant mouse PrP without the tag as an ELISA antigen. The antisera raised against mouse recombinant PrP showed only slightly higher OD_{405} values depicting antibody responses at a 100-fold dilution, compared with those of non-immunized mice (Fig. 3). In contrast, a range of much stronger antibody responses showing as higher OD_{405} values was detected with the antisera against bovine recombinant PrP (Fig. 3). The antisera against sheep recombinant PrP showed more variable titers of anti-PrP autoantibodies (Fig. 3). One mouse elicited the highest titer of anti-PrP autoantibodies among the immunized mice, but another mouse exhibited a very weak antibody response showing OD_{405} values as low as those from mouse recombinant PrP-immunized mice (Fig. 3).

3.4. Anti-bovine and anti-sheep PrP antisera recognize prion epitopes

Mouse PrP residues 91–110, 144–152, and 146–159 are the targets for protective monoclonal antibodies, ICSN 35, 6H4 and ICSN 18, respectively [9,10]. Thus, we investigated whether the antisera against bovine and sheep recombinant PrPs could recognize these epitopes. Two different mouse PrP peptides, moPrP90–109 and moPrP131–154, were synthesized and subjected to a more sensitive ELISA with each concentrated (20×) antiserum of the four to five immunized mice of each group because the conventional ELISA described above was less sensitive for detecting the specific signals. This sensitive ELISA resulted in higher backgrounds from non-immunized sera (Fig. 4). However, these two peptides were recognized with the anti-bovine and the anti-sheep PrP sera, showing higher OD_{450} values compared to non-immunized sera (Fig. 4).

Mouse PrP residues 220–231 form target epitopes for PrP-specific Fab fragments, termed R1 and R2, both of which are capable of clearing PrP^{Sc} from prion-infected N2a neuroblastoma cells [12]. We similarly performed the ELISA with a synthetic moPrP219–231 peptide (Fig. 3). Higher specific absorbance could be detected in the anti-bovine and anti-sheep sera, compared to non-immunized sera. However, we could not detect any therapeutic effects of these antisera using prion infected N2a cells (data not shown). This is probably due to very low titers of the antibodies against the peptide in these antisera, as the specific signals were undetectable by conventional ELISA.

4. Discussion

In the present study, we showed that BALB/c mice immunized with bovine recombinant PrP exhibited slightly but significantly extended survival after peripheral infection with the mouse-adapted Fukuoka-1 prion. In contrast, we could not detect any prophylactic effects against the prion in mice immunized with mouse recombinant PrP. Instead, the disease seemed to be accelerated in most of the immunized mice. Sheep recombinant PrP had variable effectiveness against the prion infection. Five out of seven immunized mice developed the disease later than non-immunized mice. However, the disease seemed to be exacerbated in two remaining mice with incubation times as short as those of mice immunized with mouse recombinant PrP. These results indicate that immu-

nization effects of recombinant bovine, sheep, and mouse PrPs on the prion infection were different in BALB/c mice.

We showed that heterologous bovine and sheep recombinant PrPs, but not mouse PrP, were immunogenic in mice, stimulating antibody responses against the respective immunizing antigens. Interestingly, we also showed that mice immunized with bovine and sheep recombinant PrPs variably produced a considerable amount of anti-PrP autoantibodies, and that these anti-PrP autoantibodies could react with the mouse PrP epitopes, moPrP90–109, moPrP131–154, and moPrP219–231. White et al. showed that passive immunization of mice with anti-PrP antibodies, which recognize the epitopes overlapping the two former epitopes, moPrP90–109 and moPrP131–154, efficiently blocked prion infection [10]. It has been also reported that titers of anti-PrP autoantibodies, which were induced by immunization with mouse recombinant PrP, were well correlated to the onset time of disease in mice inoculated with mouse 139A prion [13]. It is therefore likely that autoantibody-mediated humoral immunity could be associated with the attenuation of the Fukuoka-1 prion in mice immunized with bovine and sheep recombinant PrPs. However, at the present time, we do not know the exact mechanism of the protective effects of bovine and sheep recombinant PrP immunization on prion infection. It was reported that a cytotoxic T cell-like clone could be isolated by immunization of PrP-null mice with a PrP-derived peptide conjugated with keyhole limpet hemocyanin [14]. This might indicate an alternative possibility that cellular immunity may be involved in protection against prion infection.

The prophylactic effects of the immunization of mice with recombinant sheep PrP on the prion infection seemed variable, compared with those of recombinant bovine PrP. Western blotting of bovine PrP^C with the anti-bovine PrP sera revealed that specific antibody responses were variable in the mice immunized with bovine recombinant PrP. Mice immunized with sheep recombinant PrP also showed variable antibody responses. The titers of anti-PrP autoantibodies were also various in amounts in the mice immunized with sheep or bovine recombinant PrP but seemed more variable in the mice with recombinant sheep PrP than in the mice with recombinant bovine PrP. One mouse immunized with recombinant sheep PrP elicited very weak autoantibody responses, showing OD_{405} values as low as those of mice immunized with recombinant mouse PrP, while the other mouse produced anti-PrP autoantibodies higher than any mice immunized with recombinant PrP. Moreover, on Western blotting, specific antibody responses seemed weaker in the mice immunized with sheep PrP than in the mice immunized with bovine PrP. The titers of anti-mouse PrP autoantibodies also seemed lower and autoantibodies against moPrP90–109 and moPrP219–231 were significantly less produced in the mice with recombinant sheep PrP than in the mice with bovine recombinant PrP. It is therefore suggested that this more variable and lower amount of anti-PrP autoantibodies may reflect variable and less effective protection from the disease in mice immunized with recombinant sheep PrP, compared with that of the mice immunized with bovine recombinant PrP. However, unfortunately, because we did not individually identify the immunized mice, we could not directly compare the autoantibody titers to length of the incubation times in mice immunized with recombinant bovine and sheep PrPs in the present study. Thus, at this point, we are unable to directly answer the question why the immunization effects of recombinant sheep PrP on the prion infection were more variable than those of recombinant bovine PrP or why the two mice immunized with sheep recombinant PrP succumbed to the disease earlier than control non-immunized mice.

The disease also seemed to be exacerbated in the mice immunized with mouse recombinant PrP. It was reported that complement components C3 and C1q mediate the initial trapping of prions in lymphoreticular tissues [15,16]. Therefore, complement components, which might be upregulated by immunization, may be associated with the slight, but not significant, exacerbation of the disease. Alternatively, certain conditions induced in the peritoneal cavity by multiple immunizations could be considered to be involved in the disease exacerbation because the prion was inoculated into the same peritoneal cavity. However, these remain to be elucidated.

It was previously shown that recombinant mouse PrP was immunogenic eliciting anti-PrP autoantibodies in CD-1 mice and could slightly retard onset of the disease in immunized mice after inoculation with a mouse-adapted 139A prion [13]. However, we detected only a very weak antibody response in BALB/c mice immunized with mouse recombinant PrP and no such prophylactic effects of the immunization on the prion infection. Polymenidou et al. also reported that recombinant mouse PrP failed to induce anti-PrP autoantibodies in C57BL/6× 129Sv mice [17]. The different genetic background of mice used in each experiment may be responsible for the different antibody responses. Gilch et al. reported successfully inducing anti-PrP autoantibodies by immunization of mice with mouse recombinant PrP [18]. In this case, the recombinant PrP was inserted by a human or hamster-derived 3F4 epitope at the corresponding region, resulting in the recombinant PrP with two different amino acids from mouse PrP [18]. Thus, the recombinant PrP might acquire heterologous PrP-like immunogenicities in part and thereby induce anti-PrP autoantibodies in mice.

Molecular mimicry between microbial and host antigens is a well-known hypothetical mechanism for triggering autoimmune diseases via production of autoantibodies and/or autoreactive T cells [19,20]. This hypothesis postulates that shared identical amino acid sequences or homologous but non-identical amino acid sequences between microbial and host antigens could be essential for the initial processes of molecular mimicry [19,20]. PrPs are highly conserved molecules among mammals, sharing marked similarities in both amino acid sequence and tertiary structure [21–23]. Bovine and sheep recombinant PrPs contain 19 and 21 amino acids different from mouse recombinant PrP, respectively, indicating that the higher immunogenicity of bovine and

sheep recombinant PrPs in mice might be attributable to these different amino acids. About half of these different amino acids in bovine and sheep PrPs are concentrated in the regions corresponding to moPrP90–109, moPrP131–154, and moPrP219–231. Bovine and sheep PrPs possess 2 and 3, 4 and 3, and 4 and 4 different amino acids in the corresponding moPrP90–109, moPrP131–154, and moPrP219–231 regions, respectively. It is therefore possible that these regions of bovine and sheep PrPs are immunogenic in mice because of the different amino acid composition, eliciting antibodies, which were not only specific to themselves but also to the corresponding mouse epitopes. In other words, heterologous bovine and sheep PrPs might mimic host mouse PrP to overcome tolerance. Taken together, our present results might open a new avenue for development of molecular mimicry-based prion vaccines.

Acknowledgments

We all thank Prof. Motohiro Horiuchi (Hokkaido University) for providing a cloned bovine PrP cDNA and a cloned sheep genomic PrP DNAs. This study is partly supported by a Research on Specific Diseases from the Ministry of Health, Labour and Welfare, Japan.

References

[1] Prusiner SB. Prions. Proc Natl Acad Sci USA 1998;95(23):13363–83.
[2] Weissmann C, Enari M, Klohn PC, Rossi D, Flechsig E. Molecular biology of prions. Acta Neurobiol Exp (Wars) 2002;62(3):153–66.
[3] Wilesmith JW, Wells GA, Cranwell MP, Ryan JB. Bovine spongiform encephalopathy: epidemiological studies. Vet Rec 1988; 123(25):638–44.
[4] Hill AF, Desbruslais M, Joiner S, et al. The same prion strain causes vCJD and BSE. Nature 1997;389(6650), 448–50, 526.
[5] Bruce ME, Will RG, Ironside JW, et al. Transmissions to mice indicate that 'new variant' CJD is caused by the BSE agent. Nature 1997;389(6650):498–501.
[6] Llewelyn CA, Hewitt PE, Knight RSG, et al. Possible transmission of variant Creutzfeldt–Jakob disease by blood transfusion. Lancet 2004;363:417–21.
[7] Peden AH, Head MW, Ritchie DL, Bell JE, Ironside JW. Preclinical vCJD after blood transfusion in a PRNP codon 129 heterozygous patient. Lancet 2004;364:527–9.
[8] Gabizon R, McKinley MP, Groth D, Prusiner SB. Immunoaffinity purification and neutralization of scrapie prion infectivity. Proc Natl Acad Sci USA 1988;85(18):6617–21.
[9] Heppner FL, Musahl C, Arrighi I, et al. Prevention of scrapie pathogenesis by transgenic expression of anti-prion protein antibodies. Science 2001;294(5540):178–82.
[10] White AR, Enever P, Tayebi M, et al. Monoclonal antibodies inhibit prion replication and delay the development of prion disease. Nature 2003;422(6927):80–3.
[11] Tateishi J, Ohta M, Koga M, Sato Y, Kuroiwa Y. Transmission of chronic spongiform encephalopathy with kuru plaques from humans to small rodents. Ann Neurol 1979;5(6):581–4.
[12] Peretz D, Williamson RA, Kaneko K, et al. Antibodies inhibit prion propagation and clear cell cultures of prion infectivity. Nature 2001;412(6848):739–43.
[13] Sigurdsson EM, Brown DR, Daniels M, et al. Immunization delays the onset of prion disease in mice. Am J Pathol 2002;161(1):13–7.
[14] Bainbridge J, Walker B. Cell mediated immune responses against human prion protein. Clin Exp Immunol 2003;133(3):310–7.
[15] Mabbott NA, Bruce ME, Botto M, Walport MJ, Pepys MB. Temporary depletion of complement component C3 or genetic deficiency of C1q significantly delays onset of scrapie. Nat Med 2001;7(4):485–7.
[16] Klein MA, Kaeser PS, Schwarz P, et al. Complement facilitates early prion pathogenesis. Nat Med 2001;7(4):488–92.
[17] Polymenidou M, Heppner FL, Pellicioli EC, et al. Humoral immune response to native eukaryotic prion protein correlates with anti-prion protection. Proc Natl Acad Sci USA 2004;101:14670–6.
[18] Gilch S, Wopfner F, Renner-Muller I, et al. Polyclonal anti-PrP auto-antibodies induced with dimeric PrP interfere efficiently with PrPSc propagation in prion-infected cells. J Biol Chem 2003;278(20):18524–31.
[19] Behar SM, Porcelli SA. Mechanisms of autoimmune disease induction. The role of the immune response to microbial pathogens. Arthritis Rheum 1995;38(4):458–76.
[20] Ang CW, Jacobs BC, Laman JD. The Guillain–Barre syndrome: a true case of molecular mimicry. Trends Immunol 2004;25(2):61–6.
[21] Schatzl HM, Da Costa M, Taylor L, Cohen FE, Prusiner SB. Prion protein gene variation among primates. J Mol Biol 1997;265(2): 257.
[22] Donne DG, Viles JH, Groth D, et al. Structure of the recombinant full-length hamster prion protein PrP(29–231): the N terminus is highly flexible. Proc Natl Acad Sci USA 1997;94(25):13452–7.
[23] Riek R, Hornemann S, Wider G, Glockshuber R, Wuthrich K. NMR characterization of the full-length recombinant murine prion protein, mPrP(23–231). FEBS Lett 1997;413(2):282–8.

Available online at www.sciencedirect.com
ScienceDirect
Gene 386 (2007) 139–146
GENE
SECTION
FUNCTIONAL GENOMICS
www.elsevier.com/locate/gene

Newly established *in vitro* system with fluorescent proteins shows that abnormal expression of downstream prion protein-like protein in mice is probably due to functional disconnection between splicing and 3′ formation of prion protein pre-mRNA

Daisuke Yoshikawa [a], Juraj Kopacek [a,b], Naohiro Yamaguchi [a], Daisuke Ishibashi [c], Hitoki Yamanaka [c], Yoshitaka Yamaguchi [c], Shigeru Katamine [a], Suehiro Sakaguchi [a,c,d,*]

[a] *Department of Molecular Microbiology and Immunology, Nagasaki University Graduate School of Biomedical Sciences, Sakamoto 1-12-4, Nagasaki 852-8523, Japan*
[b] *Department of Molecular Biology, Institute of Virology, Slovak Academy of Sciences, Bratislava, Slovakia*
[c] *PRESTO Japan Science and Technology Agency, 4-1-8 Honcho Kawaguchi, Saitama, Japan*
[d] *Division of Molecular Cytology, Institute for Enzyme Research, The University of Tokushima, 3-18-15 Kuramoto-cho, Tokushima 770-8503, Japan*

Received 10 July 2006; received in revised form 8 August 2006; accepted 25 August 2006
Available online 15 September 2006
Received by A. Bernardi

Abstract

We and others previously showed that, in some lines of prion protein (PrP)-knockout mice, the downstream PrP-like protein (PrPLP/Dpl) was abnormally expressed in brains partly due to impaired cleavage/polyadenylation of the residual PrP promoter-driven pre-mRNA despite the presence of a poly(A) signal. In this study, we newly established an *in vitro* transient transfection system in which abnormal expression of PrPLP/Dpl can be visualized by expression of the green fluorescence protein, EGFP, in cultured cells. No EGFP was detected in cells transfected by a vector carrying a PrP genomic fragment including the region targeted in the knockout mice intact upstream of the PrPLP/Dpl gene. In contrast, deletion of the targeted region from the vector caused expression of EGFP. By employing this system with other vectors carrying various deletions or point mutations in the targeted region, we identified that disruption of the splicing elements in the PrP terminal intron caused the expression of EGFP. Recent lines of evidence indicate that terminal intron splicing and cleavage/polyadenylation of pre-mRNA are functionally linked to each other. Taken together, our newly established system shows that the abnormal expression of PrPLP/Dpl in PrP-knockout mice caused by the impaired cleavage/polyadenylation of the PrP promoter-driven pre-mRNA is due to the functional dissociation between the pre-mRNA machineries, in particular those of cleavage/polyadenylation and splicing. Our newly established *in vitro* system, in which the functional dissociation between the pre-mRNA machineries can be visualized by EGFP green fluorescence, may be useful for studies of the functional connection of pre-mRNA machineries.

Keywords: Intergenic splicing; *In vitro* system; Purkinje cell degeneration; Fluorescent protein

1. Introduction

Prnd is a recently identified gene encoding the first prion protein (PrP)-like protein, PrPLP/Doppel (Dpl), locating 16-kb downstream of the PrP gene, *Prnp* (Moore et al., 1999; Li et al., 2000a). *Prnd* is actively expressed in the testis, heart, skeletal muscle, and spleen, but not in the brain, whereas *Prnp* is the most abundantly expressed in the brain (Li et al., 2000b). Male mice devoid of PrPLP/Dpl were shown to be infertile due to

Abbreviations: PrP, prion protein; PrPLP/Dpl, PrP-like protein/Doppel; bp, base pair; PCR, polymerase chain reaction; nt, nucleotides; EGFP, enhanced green fluorescence protein; UTR, untranslated region; ORF, open reading frame; DMEM, Dulbecco's Modified Eagle Medium; RACE, rapid amplification of cDNA ends; HCMV, human cytomegalovirus; RNP, ribonucleoprotein; PAP, poly(A) polymerase; CPSF, cleavage/polyadenylation specificity factor.

* Corresponding author. Division of Molecular Cytology, Institute for Enzyme Research, The University of Tokushima, 3-18-15 Kuramoto-cho, Tokushima 770-8503, Japan. Tel.: +81 88 633 7438; fax: +81 88 633 7440.
E-mail address: sakaguch@ier.tokushima-u.ac.jp (S. Sakaguchi).

0378-1119/$ - see front matter © 2006 Elsevier B.V. All rights reserved.
doi:10.1016/j.gene.2006.08.028

abnormal development of sperm, indicating that PrPLP/Dpl is important for spermatogenesis (Behrens et al., 2002).

We and others found that PrPLP/Dpl is toxic when ectopically expressed in neurons deficient for the cellular PrP (PrP^C) (Moore et al., 2001; Anderson et al., 2004; Yamaguchi et al., 2004). Some lines of mice devoid of PrP^C ($Prnp^{0/0}$), including Ngsk $Prnp^{0/0}$, Rcm0 $Prnp^{0/0}$, and Zrch II $Prnp^{0/0}$, developed ataxia and Purkinje cell degeneration due to the ectopic expression of PrPLP/Dpl in neurons, but others, such as Zrch I $Prnp^{0/0}$ and Npu $Prnp^{0/0}$, showed neither the ectopic expression of PrPLP/Dpl nor such neurological abnormalities (Bueler et al., 1992; Manson et al., 1994; Sakaguchi et al., 1996; Moore et al., 1999; Rossi et al., 2001). In the ataxic lines of $Prnp^{0/0}$ mice, *Prnd* was aberrantly regulated under the control of *Prnp* promoter and thereby ectopically expressed in the brain, especially in neurons, where the *Prnp* promoter is very active (Moore et al., 1999; Li et al., 2000a). The ectopically expressing PrPLP/Dpl mRNAs were chimeric, comprising the residual *Prnp* non-coding exons 1 and 2 at the 5′ end followed by the *Prnd*-coding exons, due to an abnormal intergenic splicing taking place between *Prnp* and *Prnd* (Moore et al., 1999; Li et al., 2000a). The mechanism of how *Prnd* became abnormally regulated under the control of the *Prnp* promoter in the ataxic lines of $Prnp^{0/0}$ mice remains to be studied.

In wild-type mice, PrP pre-mRNA is normally cleaved and polyadenylated at the end of *Prnp*. However, in ataxic lines of $Prnp^{0/0}$ mice, the pre-mRNA was unsuccessfully cleaved and polyadenylated at the end of *Prnp*, resulting in its elongation until the end of downstream *Prnd* (Moore et al., 1999; Li et al., 2000a), indicating that the abnormal regulation of *Prnd* in these mice could be in part attributable to the impaired cleavage/polyadenylation of *Prnp* pre-mRNA. A polyadenylation signal is essential for the pre-mRNA cleavage/polyadenylation processes. However, the polyadenylation signal of *Prnp* and its flanking sequences are intact in two ataxic lines of Ngsk $Prnp^{0/0}$ and Rcm0 $Prnp^{0/0}$ mice. It is recently believed that the pre-mRNA processes, including acquisition of a cap structure at the 5′ end, splicing out of introns, and cleavage/polyadenylation at the 3′ end, are functionally linked to each other during transcription (Steinmetz, 1997; Proudfoot et al., 2002; Kornblihtt et al., 2004). In particular, the cleavage/polyadenylation processes are strongly influenced by splicing of the terminal intron. In the ataxic lines of $Prnp^{0/0}$ mice, a part of the *Prnp* terminal intron including the elements important for splicing, such as a splice branch point, a polypyrimidine tract, and a splice acceptor, is commonly targeted as well as the subsequent half of the last exon (Sakaguchi et al., 1995; Moore et al., 1999; Rossi et al., 2001). Thus, disruption of these splicing elements due to deletion of intron 2 could cause functional dissociation between splicing and cleavage/polyadenylation for the *Prnp* pre-mRNA in the ataxic lines of $Prnp^{0/0}$ mice, resulting in the impaired cleavage/polyadenylation of the pre-mRNA. It is alternatively possible that deletion of the exonic sequences in *Prnp* might disturb the cleavage/polyadenylation processes for the *Prnp* pre-mRNA.

In the present study, we established an *in vitro* transient transfection system in which abnormal expression of PrPLP/Dpl can be visualized by expression of the green fluorescence protein, EGFP, in cultured cells. Using this system, we identified that the abnormal expression of PrPLP/Dpl could be attributed to the functional disconnection between splicing and cleavage/polyadenylation processes. These results indicate usefulness of our newly established *in vitro* system for studying the functional connection of pre-mRNA machineries because the functional dissociation between the pre-mRNA machineries can be easily visualized by EGFP green fluorescence.

2. Materials and methods

2.1. Expression vectors

2.1.1. pPrPwild

The 488- and 2688-bp genomic fragments of *Prnd*, spanning nucleotides (nt) 35,716 to 36,204 (GenBank accession no. *U29187*) and nt 36,712 to 39,400, respectively, were first amplified from mouse genomic DNA using polymerase chain reaction (PCR; Advantage cDNA PCR KIT, Clontech, California, USA) with appropriate sets of a primer pair. The former, corresponding to a part of intron 1 and an entire 5′ untranslated region (UTR) of *Prnd*, possessed the *Sal* I and *Nhe* I enzyme sites at the 5′ and 3′ ends, respectively. The latter, consisting of an entire 3′ UTR and the downstream intervening sequence, had the *Bam*H I and *Mlu* I sites at its 5′ and 3′ ends, respectively. These fragments were ligated with the enhanced green fluorescence protein (EGFP)-coding *Nhe* I–*Bam*H I insert of pEGFP-C1 (Clontech) in such a way that the EGFP insert was flanked by the genomic fragments, and cloned into the *Sal* I and *Mlu* I sites of a pDON-AI plasmid (Takara, Tokyo, Japan) with a newly created *Mlu* I site at the multiple cloning site, yielding the plasmid pPrnd-EGFP. Next, two *Prnp* genomic DNAs, the 806-bp fragment from nt 18,861 to 19,667 encompassing a part of intron 2 and an entire 5′ UTR of exon 3 and the 1699-bp DNA from nt 20,442 to 22,140 consisting of an entire 3′ UTR and the downstream intervening sequence, were amplified by PCR. The former possessed the artificial *Spe* I and *Bam*H I enzyme sites at the 5′ and 3′ ends, respectively, and the latter contained the *Not* I and *Sal* I sites at the 5′ and 3′ ends, respectively. These fragments were ligated with the DsRed-coding *Bam*H I–*Not* I insert of pDsRed1-N1 (Clontech) in such a way that the insert was flanked by the two genomic fragments, and cloned into the *Spe* I and *Sal* I sites of pPrnd-EGFP, resulting in pPrPwild.

2.1.2. pPrP5′targeted

The 750-bp (from nt 18,661 to 19,411) fragment of *Prnp* intron 2, containing *Spe* I and *BamH* I sites at the 5′ and 3′ ends, respectively, was generated by PCR with a primer pair, and then placed for the corresponding fragment in pPrPwild, resulting in pPrP5′targeted.

2.1.3. pPrPint2(-3), pPrPint2(-26), pPrPint2(-50)

The *Prnp* intron 2 containing either 3-bp from nt 19,664 to 19,666, 26-bp from nt 19,641 to 19,666, or 50-bp from nt 19,617 to 19,666, together with the 5′ UTR of exon 3 and the

DsRed open reading frame (ORF), was amplified by PCR with a primer pair using pPrPwild as a template. *Bgl* II and *Not* I sites were introduced at the 5′ and 3′ ends of each fragment, respectively. These amplified fragments were placed for the corresponding fragment in pPrP5′targeted, respectively, yielding pPrPint2(-3), pPrPint2(-26) and pPrPint2(-50).

2.1.4. pPrP3′targeted and pPrPtargeted

A genomic fragment from nt 20,893 (corresponding to the *Eco*R I site in *Prnp* exon 3) to 22,140, encompassing a part of 3′ UTR and the downstream intervening sequence, was amplified by PCR using pPrPwild as a template with primers, each containing the *Not* I or *Sal* I recognition sequences. This amplified fragment was placed for the corresponding *Not* I–*Sal* I fragment in pPrPwild, producing a pPrP3′targeted plasmid. Moreover, pPrPtargeted was constructed by replacing this amplified fragment with the corresponding fragment in pPrP5′ targeted.

2.1.5. pPrPint2(-26)AG, pPrPint2(-26)Br, pPrPint2(-26)Br2×, pPrPint2(-26)AGBr2×

To construct these vectors, point mutations were introduced using a QuickChange Site-Directed Mutagenesis Kit (Stratagen, La Jolla, CA) using pPrPint2(-26) as a template. The mutations were verified by DNA sequencing.

2.2. Transfection and fluorescent microscopic analysis

Plasmids were transfected into mouse neuroblastoma N2a cells, which were maintained at 37 °C under 5% CO_2 in Dulbecco's Modified Eagle Medium (DMEM) supplemented with 10% fetal bovine serum. 2×10^5 cells were plated in one well of a 6-well plate and transfected by plasmids using Lipofectamin 2000 reagent (Invitrogen life technologies, Carlsbad, CA) the next day, as recommended by the manufacturer. Cells were inspected 48 h after transfection by fluorescence microscopy.

2.3. 3′ Rapid amplification of cDNA ends (RACE)

Total RNA was isolated from the cells 48 h after transfection using a Trizol reagent (Invitrogen life technologies). 1 μg of total RNA was subjected to first strand cDNA synthesis with Oligo dT-3 sites Adaptor Primer using the 3′-Full RACE Core Set (Takara) according to the manufacturer's recommendations. The synthesized cDNAs were subsequently amplified directly by PCR using the R-U5-3* primer, 5′-AGTGATTGACTACCC GTCAGCGGGGGTC-3′, and the 3 sites Adaptor Primer, 5′-CTGATCTAGAGGTACCGGATCC-3′.

2.4. DNA sequencing

DNA sequences were determined by the chain termination reaction method using Texas Red labeled specific primers (Amersham) and the ThermoSequenase premixed cycle sequencing kit (Amersham) according to the manufacturer's recommendations.

3. Results and discussion

3.1. Establishment of an in vitro transient transfection system to easily detect abnormal expression of PrPLP/Dpl by EGFP fluorescent protein

To establish an *in vitro* transient transfection system, in which the intergenic splicing-mediated abnormal expression of PrPLP/Dpl in ataxic lines of $Prnp^{0/0}$ mice can be mimicked in cultured cells, we first constructed two expression vectors, termed pPrPwild and pPrPtargeted. pPrPwild contained a part of *Prnp* genomic DNA including 816-bp of the 3′ part of intron 2, the entire exon 3, and the 3′ intervening sequence, followed by a *Prnd* genomic fragment comprising intron 1, exon 2, intron 2, exon 3 and the 3′ intervening sequence (Fig. 1B). In this vector, transcription is engineered to start from the upstream vector-derived exon under the control of the immediate early gene promoter of human cytomegalovirus (HCMV) and terminate at the end of *Prnp* exon 3 using its native poly(A) signal (Fig. 1B). We also replaced the *Prnp*- and *Prnd*-coding sequences with those of the fluorescent proteins, DsRed and EGFP, respectively (Fig. 1B), to easily detect expression of the *Prnp*- or the *Prnd*-coding exon under fluorescence microscopy. pPrPtargeted lacks the same *Prnp* region as in the ataxic lines of $Prnp^{0/0}$ mice, including 250-bp of intron 2, 10-bp of the 5′ UTR, the entire PrP ORF, and 450-bp of the 3′ UTR (Fig. 1A and B).

We then transfected these vectors into mouse N2a neuroblastoma cells and carried out a fluorescent microscopic examination 48 h after transfection. We also characterized the transcripts expressed from the vectors in these transfected cells by a 3′ RACE cloning technique and subsequent DNA sequencing. The pPrPwild-transfected cells produced DsRed fluorescence alone (Fig. 1C). No EGFP expression could be detected in these cells (Fig. 1C). 3′ RACE of the total RNA extracted from these transfected cells revealed several distinct bands, including one major and a few minor bands, on an agarose gel (Fig. 2A). We cloned the major band and determined its DNA sequence. The major transcript consisted of the vector-derived exon and *Prnp* exon 3 followed by a poly(A) tail (Fig. 2B), indicating that transcription was started from the vector-derived exon, terminating at the end of the *Prnp* exon 3, being subjected to splicing between these two exons. In contrast, pPrPtargeted produced only green EGFP but not DsRed fluorescence in the cells (Fig. 1C). 3′ RACE of these cells produced one major and a few minor bands on an agarose gel (Fig. 2A). DNA sequencing of the major band showed that it comprised the vector-derived exon and the downstream *Prnd* exons (Fig. 2B), indicating that the pre-mRNA started from the vector-derived exon was unsuccessfully terminated at the end of the *Prnp* terminal exon 3, elongated to the *Prnd* terminal exon 3, and subsequently underwent aberrant splicing between the vector-derived exon and the *Prnd* exons 2 and 3. This abnormal processing of the pre-mRNA expressed from pPrPtargeted in N2a cells is very similar to that for the targeted *Prnp* allele in the ataxic lines of $Prnp^{0/0}$ mice (Moore et al., 1999; Li et al., 2000a), whereas the processing for the pre-mRNA in the cells transfected

by pPrPwild is similar to that in wild-type mice. These results indicate that our newly established *in vitro* transient transfection system could reproduce the abnormal expression of PrPLP/Dpl in the ataxic lines of $Prnp^{0/0}$ mice in cultured cells by expression of EGFP fluorescent protein. Since pPrPtargeted lacks the *Prnp* sequences commonly targeted in the ataxic lines of $Prnp^{0/0}$ mice (Sakaguchi et al., 1995; Moore et al., 1999; Rossi et al., 2001), it is conceivable that the abnormal expression of PrPLP/Dpl in the ataxic lines of $Prnp^{0/0}$ mice is very likely due to deletion of a *cis*-element(s) present in the commonly targeted *Prnp* sequences.

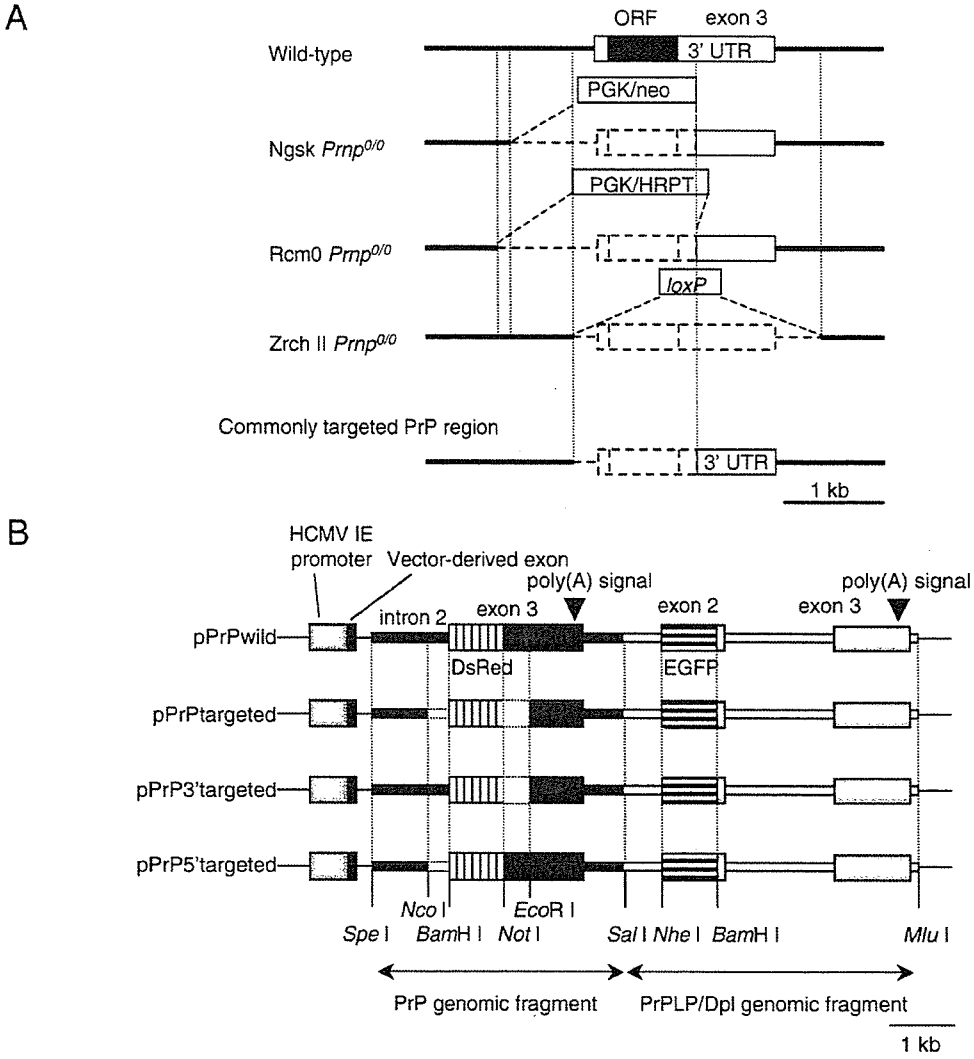

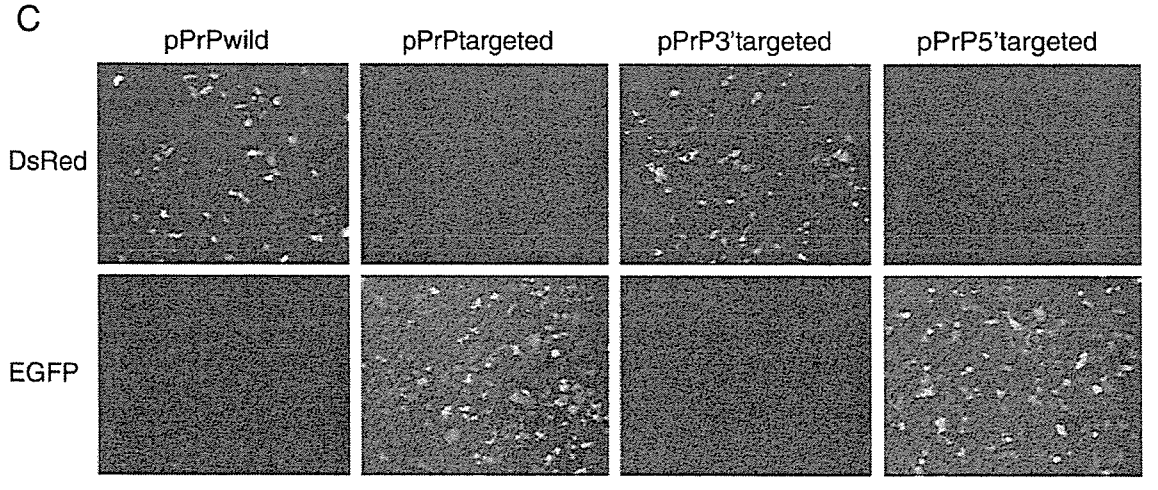

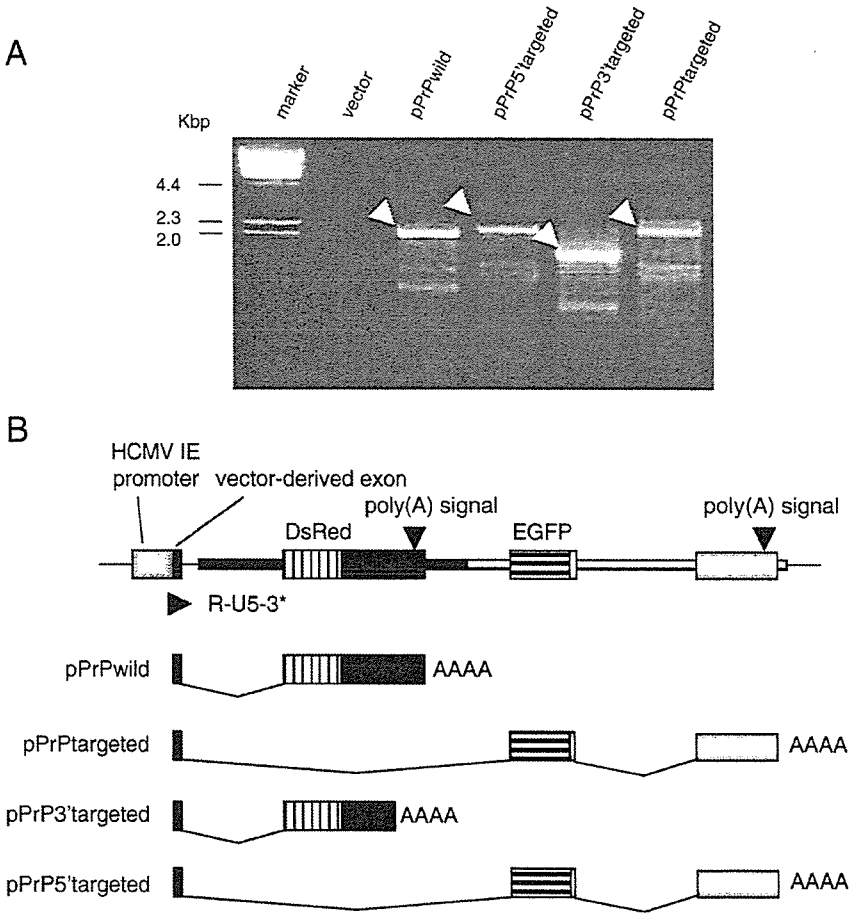

Fig. 2. (A) 3′ RACE of N2a cells 48 h after transient transfection of pPrPwild, pPrPtargeted, pPrP3′targeted, and pPrP5′targeted. Several distinct bands including one major band (indicated by arrow heads) are visible in each lane. (B) Schematic structures of the major transcripts expressed in the transfected N2a cells. These structures were determined on the basis of the DNA sequence of each major band. All poly(A) signals are native. AAAA indicates a poly(A) tail. R-U5-3* is a primer used for 3′ RACE.

3.2. Abnormal expression of PrPLP/Dpl assessed in the in vitro transient transfection system with vectors carrying various deletions in the upstream Prnp sequence

To employ our newly established *in vitro* system to investigate the genetic mechanism of the abnormal expression of PrPLP/Dpl in the ataxic lines of *Prnp*$^{0/0}$ mice, we constructed two other vectors, pPrP3′targeted and pPrP5′targeted. pPrP3′targeted lacks 450-bp of the *Prnp* 3′ UTR whereas pPrP5′targeted lacks 249-bp of intron 2 and 10-bp of the 5′ UTR (Fig. 1B). We transfected pPrP3′targeted and pPrP5′targeted into N2a cells. pPrP3′targeted expressed DsRed but not EGFP fluorescence in N2a cells 48 h after transfection (Fig. 1C). 3′ RACE and DNA sequencing showed that the major transcript expressed in these cells was composed of the vector-derived exon and the *Prnp* exon 3, similar to that in pPrPwild-transfected cells (Fig. 2A and B). This compositional similarity of the transcripts indicates that the pre-mRNAs expressed from pPrPwild and pPrP3′targeted are similarly processed in these transfected cells. Since pPrP3′targeted lacks the commonly targeted *Prnp* 3′ UTR, deletion of this part is unlikely to be involved in the

Fig. 1. (A) *Prnp* alleles in wild-type, Ngsk *Prnp*$^{0/0}$, Rcm0 *Prnp*$^{0/0}$, and Zrch II *Prnp*$^{0/0}$ mice. In Ngsk *Prnp*$^{0/0}$ mice, a 2.1-kb *Prnp* genomic DNA comprising 900-bp of intron 2, 10-bp of the 5′ UTR, an entire PrP ORF, and 450-bp of the 3′ UTR was replaced with a neomycin cassette (Sakaguchi et al., 1995). A similar part of *Prnp* was targeted in Rcm0 *Prnp*$^{0/0}$ mice (Moore et al., 1999). In Zrch II *Prnp*$^{0/0}$ mice, the *Prnp* genomic region consisting of 250-bp of intron 2, the entire exon 3, and 600-bp of the downstream intervening sequence was deleted (Rossi et al., 2001). Thus, 250-bp of intron 2 and a subsequent part of exon 3 including 10-bp of the 5′ UTR, the ORF, and 450-bp of the 3′ UTR are commonly targeted. (B) Schematic structures of the expression vectors, pPrPwild, pPrPtargeted, pPrP3′targeted, and pPrP5′targeted. pPrPwild was constructed by ligation of a PrP genomic fragment, including part of intron 2, exon 3, and the 3′ downstream sequence, and a PrPLP/Dpl genomic fragment including a part of intron 1, exon 2, intron 2, exon 3 and the 3′ downstream sequence in tandem under the control of the HCMV IE promoter. Each exon 3 contains a native poly(A) signal. The ORFs for PrP and PrPLP/Dpl are replaced with those for DsRed and EGFP, respectively. pPrPtargeted lacks the same part of *Prnp* as in the ataxic lines of *Prnp*$^{0/0}$ mice as indicated by the dotted square. pPrP3′targeted lacks 450-bp of the PrP 3′ UTR and pPrP5′targeted lacks 250-bp of intron 2 and 10-bp of the 5′ UTR. (C) Fluorescent microscopic photographs of mouse neuroblastoma N2a cells 48 h after transient transfection with pPrPwild, pPrPtargeted, pPrP3′targeted, and pPrP5′targeted.

abnormal regulation of *Prnd* in the ataxic lines of $Prnp^{0/0}$ mice. In contrast, pPrP5′targeted showed green EGFP fluorescence in the cells (Fig. 1B) and expressed the major transcript consisting of the vector-derived exon that was aberrantly spliced to the downstream *Prnd* exon 2 (Fig. 2A and B), similar to pPrPtargeted (Fig. 1B). These results indicate that our newly established *in vitro* transient transfection system is highly feasible to investigate the genetic mechanism of the abnormal expression of PrPLP/Dpl in the ataxic lines of $Prnp^{0/0}$ mice. pPrP5′targeted lacks 249-bp of intron 2 and 10-bp of the 5′ UTR. Thus, it is suggested that deletion of either 249-bp of intron 2 or 10-bp of the 5′ UTR or both in *Prnp* is responsible for the abnormal expression of downstream *Prnd* in the ataxic lines of $Prnp^{0/0}$ mice.

We further employed the *in vitro* system with several additional vectors, which were constructed by sequentially deleting 249-bp of intron 2 from the 5′ end. pPrPint2(-3) possesses only 3-bp of intron 2, including a splice acceptor of dinucleotides AG, and the subsequent 10-bp of the 5′ UTR (Fig. 3A). N2a cells transfected by this vector expressed EGFP, similar to those of pPrPtargeted and pPrP5′targeted (Fig. 3B), indicating that deletion of *Prnp* intron 2 is responsible for the abnormal expression of *Prnd*-coding exon in the transfected cells. In contrast, pPrPint2(-26) and pPrPint2(-50), containing 3′ 26- and 50-bp of intron 2, respectively, together with 10-bp of the 5′ UTR, exhibited DsRed signals in the cells (Fig. 3A and B). These results indicate that the unsuccessful cleavage/polyadenylation-mediated abnormal expression of *Prnd*-coding exon in the transfected cells is attributable to deletion of at least the 3′ 26-bp of *Prnp* intron 2. It is also suggested that lack of the same sequence in *Prnp* is responsible for the abnormal expression of PrPLP/Dpl in the ataxic lines of $Prnp^{0/0}$ mice.

3.3. The in vitro transient transfection system visualizes the functional disconnection of the pre-mRNA machineries underlying the abnormal expression of PrPLP/Dpl

Within the 26-bp intronic sequence, various elements important for pre-mRNA splicing, including a splice branch point, a polypyrimidine tract, and a splice acceptor are present. To investigate whether disruption of these elements could be involved in the impairment of pre-mRNA cleavage/polyadenylation at the end of *Prnp* leading to EGFP expression, we introduced various point mutations into the splice acceptor and/or the branch point in pPrPint2(-26). pPrPint2(-26)AG, carrying a G to T mutation in both the authentic splice acceptor AG and the adjacent downstream cryptic AG in the 5′ UTR, showed expression of EGFP in the cells (Fig. 4A and B). pPrPint2(-26)AGBr2× including mutations in all of these branch points and splice acceptors similarly expressed EGFP in the cells (Fig. 4A and B). These results clearly indicate that disruption of the splice acceptor in *Prnp* intron 2 caused expression of the downstream EGFP-coding exon. In contrast, pPrPint2(-26)Br carries an A to T mutation at the authentic branch point and expressed DsRed in the transfected N2a cells (Fig. 4A and B). Similar DsRed expression was observed in the cells transfected by pPrPint2(-26)Br2×, which contained an additional A to G mutation at the 2-bp downstream cryptic branch point (Fig. 4A and B). Therefore,

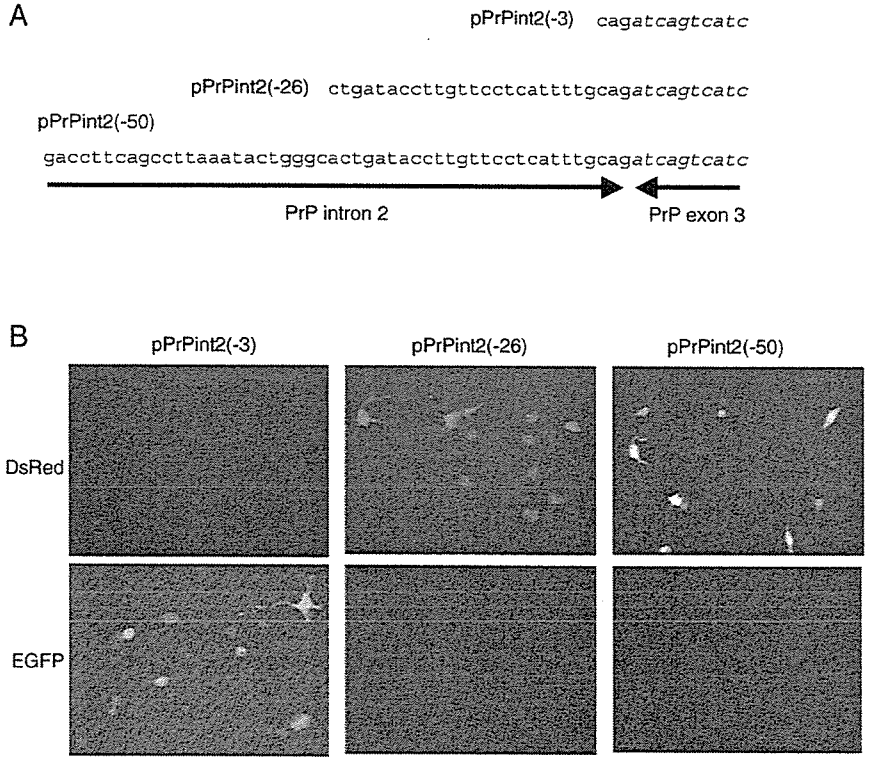

Fig. 3. (A) Nucleotide sequences of PrP intron 2 and exon 3 in pPrPint2(-3), pPrPint2(-26), and pPrPint2(-50). Italic letters are nucleotides in exon 3. (B) Fluorescent microscopic photographs of N2a cells 48 h after transient transfection with pPrPint2(-3), pPrPint2(-26), and pPrPint2(-50).

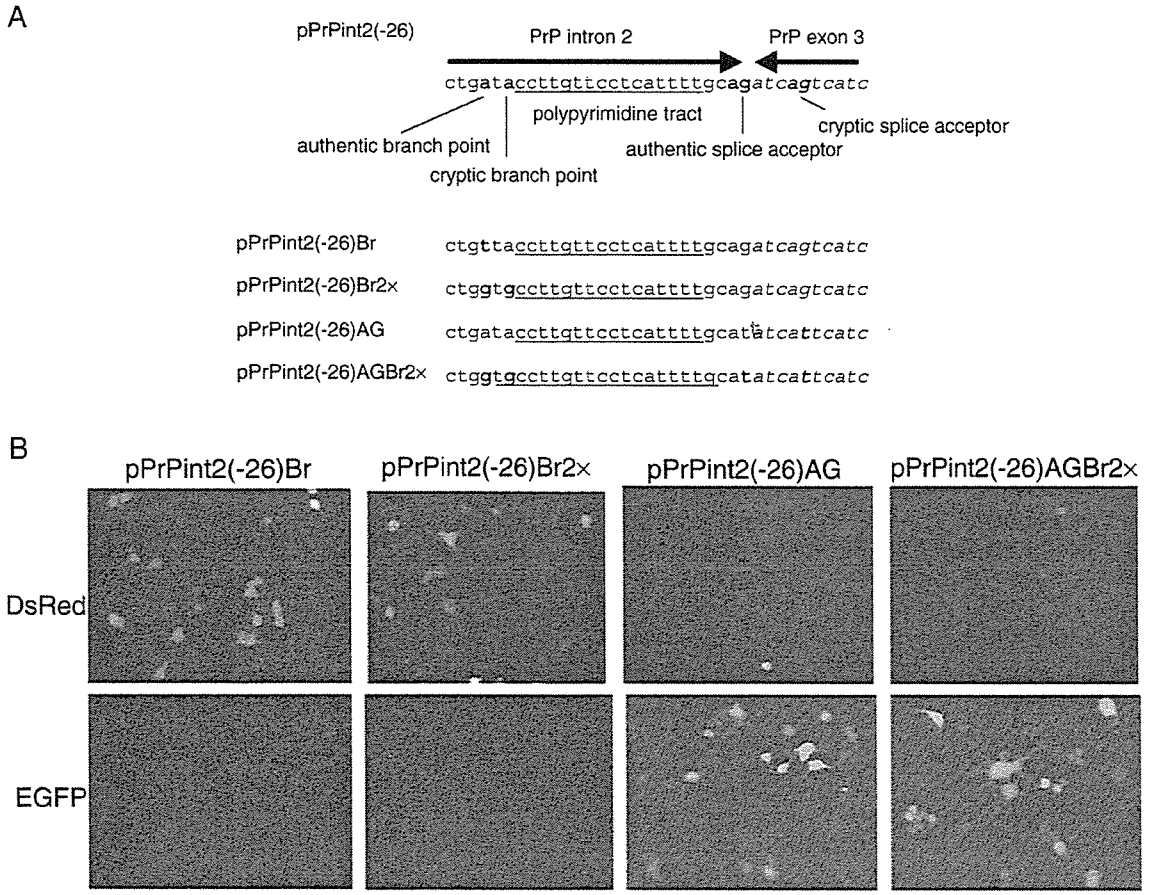

Fig. 4. (A) Point mutations introduced in the splice elements of pPrPint2(-26)Br, pPrPint2(-26)Br2×, pPrPint2(-26)AG, and pPrPint2(-26)AGBr2×. Nucleotide sequences in PrP intron 2 and exon 3 of pPrPint2(-26) are shown, including authentic and cryptic branch points, splice acceptors and a polypyrimidine tract. Mutated nucleotides are shown in bold letters. (B) Fluorescent microscopic photographs of N2a cells 48 h after transient transfection with pPrPint2(-26)Br, pPrPint2(-26)Br2×, pPrPint2(-26)AG, and pPrPint2(-26)AGBr2×.

it appears that lack of the functional branch point is unlikely to be involved in the abnormal expression of *Prnd*. However, pPrPint2(-3), which possesses the splice acceptor but lacks the branch point and polypyrimidine tract, expressed EGFP in N2a cells (Fig. 3B), indicating that deletion of the branch point or polypyrimidine tract might also be responsible for the expression of EGFP. It is thus possible that the expression of DsRed in the cells transfected by pPrPint2(-26)Br or pPrPint2(-26)Br2× is due to the presence of other functional cryptic branch points. Taken together, these results indicate that collapse in the integrity of splicing machineries could be responsible for the expression of EGFP in the cells by causing the impaired cleavage/polyadenylation of pre-mRNA. It is recently believed that splicing of the terminal intron is functionally linked to the cleavage/polyadenylation of pre-mRNA during transcription (Steinmetz, 1997; Proudfoot et al., 2002; Kornblihtt et al., 2004). It is therefore very likely that the functional disconnection of pre-mRNA machineries, in particular those of splicing and cleavage/polyadenylation, underlies the abnormal expression of PrPLP/Dpl in the ataxic lines of *Prnp*$^{0/0}$ mice. More importantly, these results indicate that our established *in vitro* transient transfection system is very useful to easily detect the functional disconnection of the pre-mRNA machineries from the expression of the EGFP fluorescent protein under fluorescence microscopy.

Splicing is mediated by a large molecular complex, splicesome, consisting of small nuclear ribonucleoproteins (snRNPs) and non-RNP splicing factors of a SR protein family (Proudfoot et al., 2002). The cleavage/polyadenylation of pre-mRNA is also regulated by various factors, including poly(A) polymerase (PAP), cleavage/polyadenylation specificity factor (CPSF), and cleavage stimulatory factor (Wahle and Ruegsegger, 1999; Proudfoot et al., 2002). U2AF is a dimeric splicing factor, interacting with the splice acceptor and polypyrimidine tract and helping recruit the U2 snRNP to the branch point together with a branch point binding protein (Vagner et al., 2000). It has been shown that PAP can interact with the large subunit of U2AF, U2AF65, and stimulate pre-mRNA splicing *in vivo* (Vagner et al., 2000). It was also reported that U2AF65 increased 3′-end cleavage efficiency (Millevoi et al., 2002). It is therefore conceivable that U2AF is a key molecule functionally connecting splicing and cleavage/polyadenylation. However, the molecular mechanism of how the pre-mRNA machineries are functionally connected to each other remains to be investigated.

Thus, our newly established *in vitro* transient transfection system might be employed to investigate the mechanism of the functional connection between the pre-mRNA machineries.

Recently, it has been shown that some viral proteins can disturb the function of pre-mRNA machineries by interacting with their components. Influenza virus NS1 protein was shown to inhibit cleavage/polyadenylation processes of cellular pre-mRNA by interacting with the 30 kDa subunit of CPSF (Nemeroff et al., 1998). Shimizu et al. subsequently reported that transcripts for the major heat shock protein HSP70, and β-actin were elongated due to the insufficient cleavage of these corresponding pre-mRNAs in influenza virus-infected cells (Shimizu et al., 1999). It was also shown that Epstein–Barr virus protein nuclear antigen 5 could inhibit cleavage/polyadenylation of cellular pre-mRNA (Dufva et al., 2002), and that human cytomegalovirus infection altered splicing and polyadenylation of cellular pre-mRNA (Adair et al., 2004). Interestingly, it was shown that Tgat, an oncogenic protein, was newly generated probably due to the impaired pre-mRNA processing in adult T-cell leukemia, the disease caused by human T-cell leukemia virus (Yoshizuka et al., 2004). Therefore, our newly established system may also be applied to elucidation of the molecular pathogenesis of pathological conditions.

3.4. Conclusions

In this study, we newly established an *in vitro* transient transfection system in which the functional disconnection of the pre-mRNA machineries could easily be detected by the expression of EGFP fluorescent protein under fluorescence microscopy. Employing this system, we showed that the abnormal expression of PrPLP/Dpl in ataxic lines of $Prnp^{0/0}$ mice can be visualized by expression of the green fluorescence protein EGFP in cultured cells, and identified that the abnormal expression of PrPLP/Dpl is probably due to functional disconnection between the pre-mRNA machineries, in particular those of splicing and cleavage/polyadenylation. Therefore, our newly established *in vitro* system might be useful to investigate the molecular mechanisms of the functional connection between the pre-mRNA machineries in normal and pathological conditions.

Acknowledgement

This study was supported in part by a Research on Specific Diseases grant from the Ministry of Health, Labour and Welfare, Japan.

References

Adair, R., Liebisch, G.W., Su, Y., Colberg-Poley, A.M., 2004. Alteration of cellular RNA splicing and polyadenylation machineries during productive human cytomegalovirus infection. J. Gen. Virol. 85, 3541–3553.

Anderson, L., Rossi, D., Linehan, J., Brandner, S., Weissmann, C., 2004. Transgene-driven expression of the Doppel protein in Purkinje cells causes Purkinje cell degeneration and motor impairment. Proc. Natl. Acad. Sci. U. S. A. 101, 3644–3649.

Behrens, A., et al., 2002. Absence of the prion protein homologue Doppel causes male sterility. EMBO J. 21, 3652–3658.

Bueler, H., et al., 1992. Normal development and behaviour of mice lacking the neuronal cell-surface PrP protein. Nature 356, 577–582.

Dufva, M., Flodin, J., Nerstedt, A., Ruetschi, U., Rymo, L., 2002. Epstein–Barr virus nuclear antigen 5 inhibits pre-mRNA cleavage and polyadenylation. Nucleic Acids Res. 30, 2131–2143.

Kornblihtt, A.R., de la Mata, M., Fededa, J.P., Munoz, M.J., Nogues, G., 2004. Multiple links between transcription and splicing. RNA 10, 1489–1498.

Li, A., et al., 2000a. Identification of a novel gene encoding a PrP-like protein expressed as chimeric transcripts fused to PrP exon 1/2 in ataxic mouse line with a disrupted PrP gene. Cell. Mol. Neurobiol. 20, 553–567.

Li, A., et al., 2000b. Physiological expression of the gene for PrP-like protein, PrPLP/Dpl, by brain endothelial cells and its ectopic expression in neurons of PrP-deficient mice ataxic due to Purkinje cell degeneration. Am. J. Pathol. 157, 1447–1452.

Manson, J.C., Clarke, A.R., Hooper, M.L., Aitchison, L., McConnell, I., Hope, J., 1994. 129/Ola mice carrying a null mutation in PrP that abolishes mRNA production are developmentally normal. Mol. Neurobiol. 8, 121–127.

Millevoi, S., Geraghty, F., Idowu, B., Tam, J.L., Antoniou, M., Vagner, S., 2002. A novel function for the U2AF 65 splicing factor in promoting pre-mRNA 3′-end processing. EMBO Rep. 3, 869–874.

Moore, R.C., et al., 1999. Ataxia in prion protein (PrP)-deficient mice is associated with upregulation of the novel PrP-like protein Doppel. J. Mol. Biol. 292, 797–817.

Moore, R.C., et al., 2001. Doppel-induced cerebellar degeneration in transgenic mice. Proc. Natl. Acad. Sci. U. S. A. 98, 15288–15293.

Nemeroff, M.E., Barabino, S.M., Li, Y., Keller, W., Krug, R.M., 1998. Influenza virus NS1 protein interacts with the cellular 30 kDa subunit of CPSF and inhibits 3′end formation of cellular pre-mRNAs. Mol. Cell 1, 991–1000.

Proudfoot, N.J., Furger, A., Dye, M.J., 2002. Integrating mRNA processing with transcription. Cell 108, 501–512.

Rossi, D., et al., 2001. Onset of ataxia and Purkinje cell loss in PrP null mice inversely correlated with Dpl level in brain. EMBO J. 20, 694–702.

Sakaguchi, S., et al., 1995. Accumulation of proteinase K-resistant prion protein (PrP) is restricted by the expression level of normal PrP in mice inoculated with a mouse-adapted strain of the Creutzfeldt–Jakob disease agent. J. Virol. 69, 7586–7592.

Sakaguchi, S., et al., 1996. Loss of cerebellar Purkinje cells in aged mice homozygous for a disrupted PrP gene. Nature 380, 528–531.

Shimizu, K., Iguchi, A., Gomyou, R., Ono, Y., 1999. Influenza virus inhibits cleavage of the HSP70 pre-mRNAs at the polyadenylation site. Virology 254, 213–219.

Steinmetz, E.J., 1997. Pre-mRNA processing and the CTD of RNA polymerase II: the tail that wags the dog? Cell 89, 491–494.

Vagner, S., Vagner, C., Mattaj, I.W., 2000. The carboxyl terminus of vertebrate poly(A) polymerase interacts with U2AF 65 to couple 3′-end processing and splicing. Genes Dev. 14, 403–413.

Wahle, E., Ruegsegger, U., 1999. 3′-End processing of pre-mRNA in eukaryotes. FEMS Microbiol. Rev. 23, 277–295.

Yamaguchi, N., Sakaguchi, S., Shigematsu, K., Okimura, N., Katamine, S., 2004. Doppel-induced Purkinje cell death is stoichiometrically abrogated by prion protein. Biochem. Biophys. Res. Commun. 319, 1247–1252.

Yoshizuka, N., et al., 2004. An alternative transcript derived from the trio locus encodes a guanosine nucleotide exchange factor with mouse cell-transforming potential. J. Biol. Chem. 279, 43998–44004.

Cellular and Molecular Neurobiology (© 2006)
DOI: 10.1007/s10571-006-9125-x

Inhibition of Transforming Growth Factor-β Production in Brain Pericytes Contributes to Cyclosporin A-Induced Dysfunction of the Blood-Brain Barrier

Fuyuko Takata,[1,2] Shinya Dohgu,[1] Atsushi Yamauchi,[1] Noriko Sumi,[1] Shinsuke Nakagawa,[2,3] Mikihiko Naito,[4] Takashi Tsuruo,[4] Hideki Shuto,[1] and Yasufumi Kataoka[1,2,5]

Received July 24, 2006; accepted October 5, 2006

SUMMARY

1. The present study was designed to clarify whether brain pericytes and pericyte-derived transforming growth factor-β1 (TGF-β1) participate in cyclosporin A (CsA)-induced dysfunction of the blood-brain barrier (BBB).

2. The presence of brain pericytes markedly aggravated CsA-increased permeability of MBEC4 cells to sodium fluorescein and accumulation of rhodamine 123 in MBEC4 cells.

3. Exposure to CsA significantly decreased the levels of TGF-β1 mRNA in brain pericytes in pericyte co-cultures. Treatment with TGF-β1 dose-dependently inhibited CsA-induced hyperpermeability and P-glycoprotein dysfunction of MBEC4 cells in pericyte co-cultures.

4. These findings suggest that an inhibition of brain pericyte-derived TGF-β1 contributes to the occurrence of CsA-induced dysfunction of the BBB.

KEY WORDS: Cyclosporin A; brain pericytes; transforming growth factor-β; blood-brain barrier; permeability; P-glycoprotein; mouse brain endothelial cells .

INTRODUCTION

Cyclosporin A (CsA), a cyclic 11-amino acid peptide, is widely used as a potent immunosuppressant to prevent allograft rejection in solid organ transplantation and in fatal graft-versus-host disease after bone marrow transplantation; it is also used to treat various autoimmune diseases including rheumatoid arthritis (Ka-

[1] Department of Pharmaceutical Care and Health Sciences, Faculty of Pharmaceutical Sciences, Fukuoka University, Jonan-ku, Fukuoka, 814-0180, Japan.
[2] PharmaCo-Cell Company Ltd., Nagayo-machi, Nagasaki, 851-2127, Japan.
[3] Department of Pharmacology 1, Nagasaki University School of Medicine, Sakamoto, Nagasaki, 852-8501, Japan.
[4] Institute of Molecular and Cellular Biosciences, University of Tokyo, Bunkyo-ku, Tokyo, 113-0032, Japan.
[5] To whom correspondence should be addressed; e-mail: ykataoka@fukuoka-u.ac.jp.

han, 1989). Despite its high efficacy, CsA has adverse effects including nephrotoxicity, cardiovascular disorders, gastrointestinal disorders and neurotoxicity. CsA-associated neurotoxicity occurs with a relatively high frequency (20–40%) in organ-transplanted patients with high blood drug levels or within the therapeutic range (The U.S. Multicenter FK506 Liver Study Group, 1994; Pirsch *et al.*, 1997; Gijtenbeek *et al.*, 1999). However, the mechanism of CsA-induced neurotoxicity remains obscure.

The entry of CsA into the brain is usually prevented by the tight junctions and P-glycoprotein (P-gp), a multi-drug efflux pump, of brain microvascular endothelial cells. But CsA-associated neurotoxicity, including tremors, seizures and encephalopathy, strongly suggests the possibility that CsA is transported across the blood-brain barrier (BBB). We previously reported that CsA produced convulsions by inhibiting γ-aminobutyric acid (GABA)ergic neural activity and the binding properties of the $GABA_A$ receptor (Shuto *et al.*, 1999). The inhibition of GABAergic neurotransmission by CsA may lead to an activation of serotonergic neural activity and, consequently, produce tremors (Shuto *et al.*, 1998). These *in vivo* findings are considered to be due to a direct action of CsA transported across the BBB rather than an indirect effect of CsA in the periphery. Indeed, we previously demonstrated that a high concentration of CsA decreased the function and expression of P-gp in brain capillary endothelial cells (Kochi *et al.*, 1999, 2000). The BBB is primarily formed from these cells, which are closely sealed by tight junctions (Pardridge, 1999). P-gp is abundantly expressed in brain endothelial cells and limits the accumulation of many hydrophobic molecules and toxic substances in the brain (Schinkel, 1999). Brain capillary endothelial cells are surrounded by two other cellular components of the BBB, astrocytes and brain pericytes. We also previously reported that the presence of astrocytes markedly aggravated CsA-induced hyperpermeability of, and P-gp dysfunction in, MBEC4 cells, through the acceleration of NO production (Dohgu *et al.*, 2004a). Brain pericytes are important for the growth and migration of endothelial cells and the integrity of microvascular capillaries (Thomas, 1999; Ramsauer *et al.*, 2002). Brain capillary endothelial cells communicate closely with brain pericytes to maintain the BBB (Hori *et al.*, 2004; Dohgu *et al.*, 2005). Transforming growth factor-β (TGF-β) is a cytokine produced by pericytes (Antonelli-Orlidge *et al.*, 1989). We previously reported that brain pericytes contribute to the up-regulation of barrier function and P-gp activity in brain endothelial cells through production of TGF-β1 (Dohgu *et al.*, 2005).

The present study was designed to clarify whether brain pericytes and pericyte-derived TGF-β participate in CsA-induced dysfunction of the BBB. We first evaluated the effect of CsA on the permeability of, and P-gp function in, mouse brain capillary endothelial (MBEC4) cells, either alone or co-cultured with human brain pericytes. Next, the effect of CsA on TGF-β1 mRNA expression in brain pericytes and the effect of TGF-β1 on CsA-decreased BBB function were examined in a co-culture system containing MBEC4 cells and brain pericytes.

MATERIALS AND METHODS

Materials

CsA was kindly supplied by Novartis Pharma (Basel, Switzerland). Sodium fluorescein (Na-F, MW 376), rhodamine 123 and human TGF-β1 were purchased from Sigma (St. Louis, MO). Culture medium and subculture reagents were obtained from Invitrogen (Carlsbad, CA). All remaining reagents of analytical grade were purchased from Wako (Osaka, Japan).

Cell Culture

MBEC4 cells, isolated from BALB/c mouse brain cortices and immortalized by SV40-transformation (Tatsuta *et al.*, 1992), were cultured in Dulbecco's modified Eagle's medium (DMEM) supplemented with 10% fetal bovine serum, 100 units/mL penicillin and 100 μg/mL streptomycin. Human brain pericytes (CS-ABI-499, Cell Systems Corporation, Kirkland, WA) were cultured in CS-C Complete Medium Kit (Cell Systems Corporation). They were grown in a humidified atmosphere of 5% CO_2/95% air at 37°C. To make an *in vitro* BBB model, brain pericytes (20,000 cells/cm^2) were first cultured in the wells of a 12-well culture plate. After 2 days, MBEC4 cells (42,000 cells/cm^2) were seeded on the inside of the collagen-coated polycarbonate membrane (1.0 cm^2, 3.0 μm pore size) of a Transwell®-Clear insert (12-well type, Costar, MA) placed in the plate containing layers of brain pericytes (pericyte co-culture). A monolayer system was also generated with MBEC4 cells alone (MBEC4 monolayer).

Cell viability was assessed using a WST-8 assay (Cell Counting Kit, DOJINDO, Kumamoto, Japan). The absorbance of a highly water-soluble formazan dye (WST-8), reduced by mitochondrial dehydrogenase, was measured in each sample at wavelengths of 450-nm (test wavelength) and 700-nm (reference wavelength).

Treatment with CsA and TGF-β1

TGF-β1 was dissolved in 4 mM HCl containing 1 mg/mL of bovine serum albumin; CsA was dissolved in ethanol. Each original solution was then diluted with serum-free medium. The final concentrations in the test media were 4 μM HCl/1 μg/mL bovine serum albumin or 0.1% ethanol. MBEC4 cells were cultured for 3 days, and the inserts were washed three times with serum-free medium. Cells were then exposed for 1–12 h to 5 μM of CsA injected into the inside of the insert (luminal side). Alternatively, TGF-β1 (0.01–1 ng/mL) was loaded on the luminal side. In parallel, cells were treated with serum-free medium containing the corresponding amount of ethanol and/or HCl and bovine serum albumin as the vehicle.

Transcellular Transport of Na-F

To initiate the transport experiments, the medium was removed and MBEC4 cells were washed three times with Krebs–Ringer buffer (118 mM NaCl, 4.7 mM KCl, 1.3 mM $CaCl_2$, 1.2 mM $MgCl_2$, 1.0 mM NaH_2PO_4, 25 mM $NaHCO_3$, and 11 mM D-glucose, pH 7.4). Krebs–Ringer buffer (1.5 mL) was added to the outside of the insert (abluminal side). Krebs–Ringer buffer (0.5 mL) containing 100 μg/mL of Na-F was loaded on the luminal side of the insert. Samples (0.5 mL) were removed from the abluminal chamber at 10, 20, 30 and 60 min and immediately replaced with fresh Krebs–Ringer buffer. Aliquots (5 μL) of the abluminal medium were mixed with 200 μL of Krebs–Ringer buffer and the concentration of Na-F was determined using a fluorescence multiwell plate reader (Ex(λ) 485 nm; Em(λ) 530 nm) (CytoFluor Series 4000, PerSeptive Biosystems, Framingham, MA). The permeability coefficient and clearance were calculated according to the method described by Dehouck *et al.* (1992). Clearance was expressed as microliters (μL) of tracer diffusing from the luminal to abluminal chamber and was calculated from the initial concentration of tracer in the luminal chamber and final concentration in the abluminal chamber: clearance (μL) = $[C]_A \times V_A/[C]_L$ where $[C]_L$ is the initial luminal tracer concentration, $[C]_A$ is the abluminal tracer concentration and V_A is the volume of the abluminal chamber. During the 60-min period of the experiment, the clearance volume increased linearly with time. The average volume cleared was plotted against time, and the slope was estimated by linear regression analysis. The slope of clearance curves for the MBEC4 monolayer or co-culture systems was denoted by PS_{app}, where PS is the permeability–surface area product (in μL/min). The slope of the clearance curve with a control membrane was denoted by $PS_{membrane}$. The real PS value for the MBEC4 monolayer and the co-culture system (PS_{trans}) was calculated as $1/PS_{app} = 1/PS_{membrane} + 1/PS_{trans}$. The PS_{trans} values were divided by the surface area of the Transwell inserts to generate the permeability coefficient (P_{trans}, in cm/min).

Functional Activity of P-gp

The functional activity of P-gp was determined by measuring the cellular accumulation of rhodamine 123 (Sigma) according to the method of Fontaine *et al.* (1996). MBEC4 cells were washed three times with assay buffer (143 mM NaCl, 4.7 mM KCl, 1.3 mM $CaCl_2$, 1.2 mM $MgCl_2$, 1.0 mM NaH_2PO_4, 10 mM HEPES, and 11 mM D-glucose, pH 7.4), and then incubated in 0.5 mL of assay buffer containing 5 μM rhodamine 123 for 60 min. The solution was then removed and the cells were washed three times with ice-cold phosphate-buffered saline and solubilized in 1 M NaOH (0.2 mL). The solution was neutralized with 1 M HCl (0.2 mL) and the rhodamine 123 content was determined using a fluorescence multiwell plate reader (Ex(λ) 485 nm; Em(λ) 530 nm, CytoFluor Series 4000). Protein concentration was measured by the method of Bradford (Bradford, 1976).

Expression of TGF-β1 Receptor mRNA in MBEC4 Cells and Human Brain Pericytes

Reverse-transcription polymerase chain reaction (RT-PCR) was employed to determine the level of mRNA expression for TGF-β1 receptor I and II in MBEC4 cells and brain pericytes. Total RNA was extracted from cultured cells using TRIzol™ reagent (Invitrogen, Carlsbad, CA) and 1 μg of RNA was reverse-transcribed and amplified by PCR using a SuperScript One-Step RT-PCR system (Invitrogen). Amplification was performed in a DNA thermal cycler (PC707; ASTEC, Fukuoka, Japan). The primers used and PCR conditions are summarized in Table I. Ten microliters of each PCR product was analyzed by electrophoresis on a 2% agarose (Sigma) gel with ethidium bromide staining. Gels were visualized on a UV light transilluminator and photographed using a DC290 Zoom digital camera (Kodak, Rochester, New York).

Relative Quantitation of TGF-β1 mRNA by Real-Time RT-PCR

Real-time RT-PCR was employed to determine the level of TGF-β1 gene expression in brain pericytes with CsA-treated pericyte co-culture. Total RNA was extracted from brain pericytes using TRIzol™ reagent (Invitrogen) and 2 μg RNA was reverse-transcribed using a SuperScript™ III First-Strand Synthesis System (Invitrogen) in a total volume of 20 μL, according to the manufacturer's protocol.

Real-time PCR was conducted on an Mx3000P™ Multiplex Quantitative PCR System (Stratagene, La Jolla, CA) with 2 μL of reverse-transcription product, Brilliant™ SYBR® Green QPCR Master Mix (Stratagene), primers at 150 nM and reference dye, in a total volume of 50 μL as per the manufacturer's protocol. The following PCR conditions were employed: 95°C for 10 min, followed by cycles of 95°C for 30 s, 54°C for 60 s and 72°C for 90 s. The sequences of primers were as follows: sense primer 5′-CCCTGGACACCAACTATTG-3′ and antisense primer 5′-CCGGGTTATGCTGGTTGTA-3′ for TGF-β1 (Untergasser *et al.*, 2005); sense primer 5′-GAGTCAACGGATTTGGTCGT-3′ and antisense primer 5′-TTGATTTTGGAGGGATCTCG-3′ for glyceraldehyde-3-phosphate dehydrogenase (GAPDH; GenBank Accession Number, M33197). After amplification, a melting curve was obtained by heating at 55°C and fluorescence data were collected at 0.2°C/s.

Relative quantitative analysis was performed employing Mx3000P™ Multiplex Quantitative PCR System software (Stratagene). We used the expression of GAPDH to normalize the expression data for the TGF-β1 gene. For a comparative analysis, values from vehicle treated brain pericytes were arbitrarily set as 1. Each sample was analyzed in triplicate.

Statistical Analysis

Values are expressed as means ± SEM. Statistical analysis was performed using Student's *t*-test. One-way and two-way analyses of variance (ANOVAs) followed by Tukey–Kramer's tests or Dunnett tests were applied to multiple com-

Table I Nucleotide Sequences of Probes Used in RT-PCR Assays and Amplification Conditions

Gene	Source (reference)	Sequence	Product (bp)	Amplification conditions
TGF-β R	Mouse (Machida *et al.*, 2000)	Sense 5′-ATCCATCACTAGATCGCCCT-3′ Antisense 5′-CGATGGATCAGAAGGTACAAGA-3′	824	94°C for 30 s, 57°C for 30 s, 72°C for 30 s
	Human (GenBank Accession Number, L11695)	Sense 5′-GATGGGCTCTGCTTTGTCTC-3′ Antisense 5′-CAAGGCCAGGTGATGACTTT-3′	214	94°C for 30 s, 54°C for 30 s, 72°C for 30 s
TGF-β R	Mouse (Machida *et al.*, 2000)	Sense 5′-CGTGTGGAGGAAGAACAACA-3′ Antisense 5′-TCTCAAACTGCTCTGAGGTG-3′	560	94°C for 30 s, 57°C for 30 s, 72°C for 30 s
	Human (GenBank Accession Number, E10743)	Sense 5′-TTTTCCACCTGTGACAACCA-3′ Antisense 5′-GGAGAAGCAGCATCTTCCAG-3′	185	94°C for 30 s, 54°C for 30 s, 72°C for 30 s

parisons. The differences between means were considered to be significant when P values were less than 0.05.

RESULTS

To obtain molecular evidence for the expression of TGF-β receptor I and II in MBEC4 cells and human brain pericytes, RT-PCR was carried out with a primer pair specific to each type of TGF-β receptor, from either mouse (for use on MBEC4 cells) or human (for use on human brain pericytes). As shown in Fig. 1A, RT-PCR with mRNA obtained from either MBEC4 cells or brain pericytes yielded a single product. The size of these products was as expected from the primer positions.

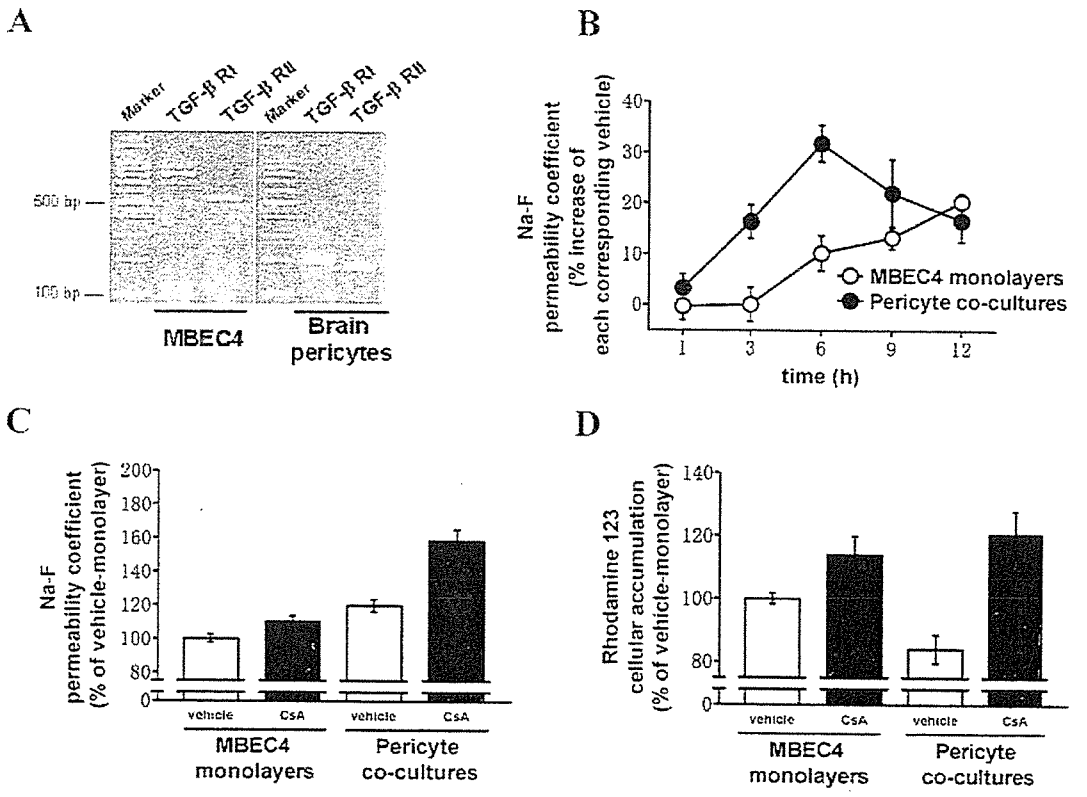

Fig. 1 (A) Expression of TGF-β receptor I and II mRNA in MBEC4 cells and human brain pericytes by RT-PCR analysis. (B) Time-course of the effect of CsA (5 μM) on the Na-F permeability of MBEC4 cells in MBEC4 monolayers and pericyte co-cultures. Transport experiments were performed after 1, 3, 6, 9 and 12 h of exposure to CsA. Results are expressed as % increase of each corresponding vehicle treatment (MBEC4 monolayers; $2.78 \pm 0.10 \times 10^{-4}$ to $3.47 \pm 0.14 \times 10^{-4}$ cm/min, pericyte co-cultures; $3.24 \pm 0.10 \times 10^{-4}$ to $4.47 \pm 0.20 \times 10^{-4}$ cm/min). Values are the means $\pm$ SEM (n = 7–16). (C) Effect of treatment with CsA (5 μM) for 6 h on the Na-F permeability of MBEC4 cells in MBEC4 monolayers and pericyte co-cultures. Results are expressed as % of vehicle-treated MBEC4 monolayers (% of vehicle-monolayer ($3.26 \pm 0.13 \times 10^{-4}$ cm/min)). Values are the means $\pm$ SEM (n = 7). (D) Effect of treatment with CsA (5 μM) for 6 h on the rhodamine 123 accumulation of MBEC4 cells in MBEC4 monolayers and pericyte co-cultures. Results are expressed as % of vehicle-treated MBEC4 monolayers (% of vehicle-monolayer (0.51 $\pm$ 0.12 nmol/mg protein)). Values are the means $\pm$ SEM (n = 8).